

Watch Me Calibrate My Force-Sensing Shoes!

Yuanfeng Han*, Boren Jiang[†] and Gregory S. Chirikjian[†]

Abstract—This letter presents a novel method for smaller-sized humanoid robots to self-calibrate their foot force sensors. This method consists of two steps: 1. The robot is commanded to move along several planned whole-body trajectories. 2. A nonlinear least-squares technique is implemented to determine sensor parameters by minimizing the error between the measured and modeled center of pressure (CoP) and ground reaction force (GRF) in the robot’s movement. This is the first proposed autonomous calibration method for foot force sensors in humanoid robots. Additionally, a manual calibration method is developed to improve the CoP measurement accuracy, which establishes the ground truth for evaluating the self-calibration approach. The manual calibration and the self-calibration are implemented on our previously presented force-sensing shoes. The results show that the self-calibration method, without any manual intervention, can accurately estimate CoP and GRF.

I. INTRODUCTION

Foot force sensors are widely used in humanoid robots for measuring GRF and CoP to determine the stability of the system [1]. Many researchers have designed planning and control algorithms for humanoid robots that incorporate foot sensory feedback in dynamic walking [2], self-balancing [3], push-and-recovery [4], etc. In addition, foot force sensors are also applied to estimate the humanoid robot’s center of mass (CoM) location [5], and external forces [6]. Recent studies use foot force sensors to identify the mass properties of heavy objects in manipulation tasks of humanoid robots [7], [8].

Two common types of foot force sensors are used to measure CoP and GRF for humanoid robots. Commercial force/torque (F/T) sensors have been widely applied to larger-sized humanoid platforms [9], [10]. Such a sensor is usually mounted between the robot’s ankle and foot. The GRF is directly measured from the sensor’s force outputs, and the CoP is obtained by solving torque balance [11]. The commercial F/T sensors, although accurate, are too expensive and heavy for smaller-sized humanoids [12]. By contrast, light-weight and low-cost force-sensing resistors (FSRs) are often adopted to construct the foot force-sensing modules by smaller-sized humanoids [13], [14]. In most of the foot designs, FSRs are distributed close to the foot’s boundary. The convex hull containing these FSRs is the allowable measurement area for CoP, which is also called sensing polygon (smaller than the robot’s support polygon) [15]. Since each FSR outputs 1-D force, the robot’s normal GRF is the total force output (see 1). The CoP is obtained by averaging the position of each sensor weighted by their

corresponding force outputs (see 2). In practice, FSRs often suffer from resistance drift and hysteresis and they are not suitable for accurate force measurement [16].

In the literature, there are three ways to enhance the measurement accuracy of the foot force-sensing modules constructed by FSRs. 1. *Improving sensor’s quality.* Researchers either developed their own light-weight force/pressure sensors with higher accuracy or customized the existing higher-quality commercial force/pressure sensors into the foot design. For example, Shayan et al. modified barometric pressure sensors to replace the poor factory default FSRs in the NAO robot’s feet [17]. Kwon et al. developed a pressure-sensing foot using custom-fabricated polymer-based pressure sensors for a KIBO robot [18]. Our proposed force-sensing shoes [19] utilize light-weight single-axis load cells for force measurement. 2. *Improving foot force-sensing module design.* For example, to improve the NAO robot’s poor foot design, in which the FSRs incompletely contact the foot bottom plate. Almeida et al. proposed a two-layer force-sensing module design facilitating all the FSRs to engage when the robot applies force on the shoes [20]. Our proposed force-sensing shoe ensures all force sensors are effectively activated by directly cantilevering the shoe’s top plate on the top of the sensors [19]. Additionally, the authors in [21] add a soft sponge layer between the FSRs and the foot bottom plate to facilitate contact for a KHR-2HV robot. 3. *Applying manual calibration.* Manual calibration includes single sensor calibration and force-sensing module calibration. The former requires applying different reference forces to the sensor and then using linear or nonlinear regressions to map out the relationship between the sensor’s voltage output and the applied force. The latter aims to improve the measurement accuracy of a specific metric incorporating all sensor outputs, of which the most common one is the CoP. Our work [19] proposed a CoP manual calibration method, which Applies known weights to designated positions on the top of the foot module and minimizes the error between the measured CoP and its ground truth over sensor parameters.

The abovementioned manual calibration methods need to be implemented frequently since force sensors drift as the environmental factor changes. For example, a change in temperature may lead to an offset on the measurements. Or slight variations in the mechanical structure during usage, such as changes in screw tension and deformations of the mounting material, may affect the measurement accuracy. However, performing manual calibration is not only time-consuming but also requires human intervention, which made it impossible for humanoid robots to use accurate force sensory feedback in long-term autonomous tasks. Therefore,

* Yuanfeng Han is with the Department of Mechanical Engineering, Johns Hopkins University, Baltimore, MD, USA yhan33@jhu.edu

[†] Gregory S. Chirikjian and Boren Jiang are with the Department of Mechanical Engineering, National University of Singapore, Singapore mpegre@nus.edu.sg

this letter demonstrates **two major contributions**:

1. We propose a novel self-calibration method for a humanoid robot to calibrate its force/pressure sensor parameters using different body configurations. Specifically, the robot reaches several sampled double-support configurations, fixes its feet, and then moves the rest of its body along with planned whole-body trajectories. Then the optimal sensor parameters are determined by minimizing the error between the measured CoP, GRF, and their modeled references using nonlinear optimization. To our best knowledge, it is the first presented autonomous method for calibrating foot sensors for humanoid robots.

2. We developed a manual calibration approach to improve the accuracy of CoP measurement, which incorporates force-plate calibration techniques. This method reduces the mean absolute error of the measured CoP to only around 1 mm. The improved CoP is used to establish the ground truth for evaluating the self-calibration approach.

The self and the manual calibrations are individual novelties to enhance foot force-sensing for humanoid robots. The former can be used for long-term autonomous tasks and the latter can be applied to short-term tasks requiring high measurement accuracy. Though the self-calibration approach is demonstrated on our force-sensing shoes designed for smaller humanoids, it can theoretically be applied to larger humanoid robots with F/T sensors as well.

II. FORCE-SENSING SHOE OVERVIEW

This section gives a brief overview of our previously presented force-sensing shoes [19].

A. Design

The shoe consists of two 3-D printed plates and measures forces using four 1-D load-cells (Fig. 1a). One side of the load cell is cantilevered at the holders of the bottom plate, and its other side connects the corners of the top plate (Fig. 1a). Slightly different from the first version design in [19], the current design includes a six-by-three array of holes on the top plate (Fig. 1a), which are directly used for manual calibration (see Section III). These holes cover the sensing polygon constructed by the NAO's factory default FSRs (Fig. 1a, grey area) [22]. This calibration area, slightly smaller than the shoe's support polygon, is the allowable CoP region for the robot's default functionalities for safety concerns.

B. Sensing principle

The shoe measures GRF and CoP. The GRF, F , is acquired by summing up all the force output f_i (Fig. 1b):

$$F = \sum_{i=1}^4 f_i. \quad (1)$$

The CoP, C , is obtained by averaging the 2-D position of each load cell in the spatial coordinate, \mathbf{t}_i , weighted by their corresponding force outputs, f_i (Fig. 1b):

$$C = \sum_{i=1}^4 f_i \mathbf{t}_i / \sum_{i=1}^4 f_i. \quad (2)$$

The sensing principle for single support can also be applied to double support by incorporating all eight sensors.

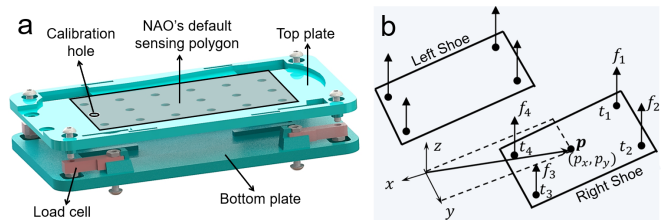


Fig. 1. (a) Shoe design. (b) Shoe's sensing principle

III. SHOE MANUAL CALIBRATION

This section introduces a manual calibration method for the shoe's CoP measurement, including *load-cell calibration* and *shoe calibration*. Although this is not the main topic of our paper, it is used to establish ground truth for evaluation of the self-calibration algorithm that will come later.

A. Load cell calibration

To calibrate each load cell, we first record its no-load voltage S_0 (Fig. 3a, left) and then record the updated voltage S_G after applying a known mass G to the sensor (Fig. 3a, right). Due to the load cell's linear response between the voltage output and the applied force, the voltage to force ratio $\sigma = (S_G - S_0)/G$. Then, the force output F corresponding to a loaded voltage output S is given by:

$$F = (S - S_0)/\sigma = aS + b, \quad (3)$$

where a and b are the modified scaling factor and offset.

B. Shoe calibration

As introduced in [19], our force-sensing shoes possess high accuracy in GRF measurement (Fig. 2a) but low accuracy in CoP measurements (Fig. 2b and c, left). To improve the CoP measurement accuracy, we applied seven different weights (1, 1.5, 2, 2.5, 3, 3.5, 4kg masses $\approx 18\%$, 27% , 37% , 46% , 55% , 64% , 73% of the robot's weight) to the three-by-eight array of holes on the shoe's top plate through a 3-D printed support (Fig. 3b). Then, we applied nonlinear least squares to minimize the error between measured CoP and their corresponding ground truths, which are the known positions of the holes.

Inspired by a force plate calibration method introduced in [23], our manual calibration defines a corrected CoP, $[p_x, p_y]^T$, by summing the measured CoP $[p_{0x}, p_{0y}]^T$ and a correction term $[\Delta x, \Delta y]^T$:

$$\begin{bmatrix} p_x \\ p_y \end{bmatrix} = \begin{bmatrix} p_{0x} \\ p_{0y} \end{bmatrix} + \begin{bmatrix} \Delta x \\ \Delta y \end{bmatrix}. \quad (4)$$

The correction term is formulated as :

$$\begin{bmatrix} \Delta x \\ \Delta y \end{bmatrix} = \begin{bmatrix} a_1 p_{0x}^2 + a_2 p_{0x} + a_3 p_{0y} + a_4 + \sum_{i=1}^4 m_i f_i \\ b_1 p_{0y}^2 + b_2 p_{0y} + b_3 p_{0x} + b_4 + \sum_{i=1}^4 n_i f_i \end{bmatrix}, \quad (5)$$

where Δx is designed using a second-order and a first-order polynomials of the measured CoP's x and y coordinates. This part is used to improve the averaged measurement at each calibration hole according to the work [23]. Δx also includes a first-order term of the force outputs to reduce the

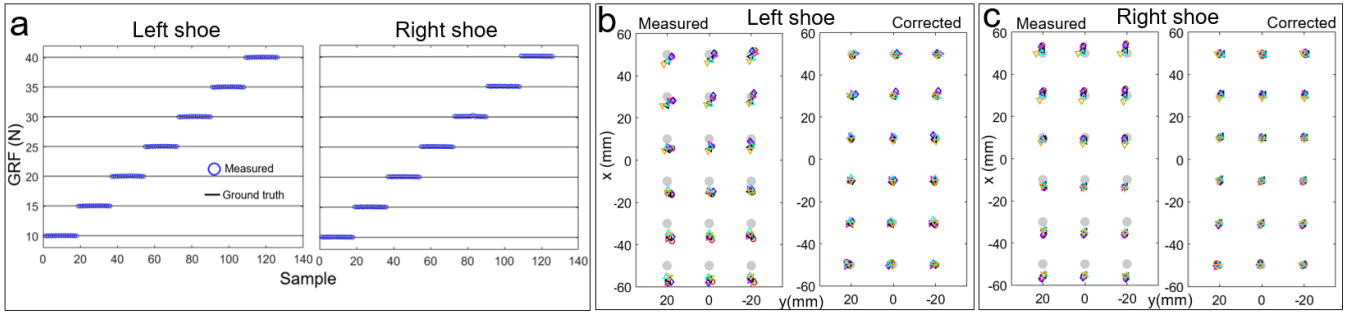


Fig. 2. (a) Measured GRF (blue circles) and their ground truths (black lines). (b) (c) Measured CoP (left) and the corrected CoP (right) for the left and the right shoes. Colored markers represent different weights and grey circles are their corresponding ground truths.

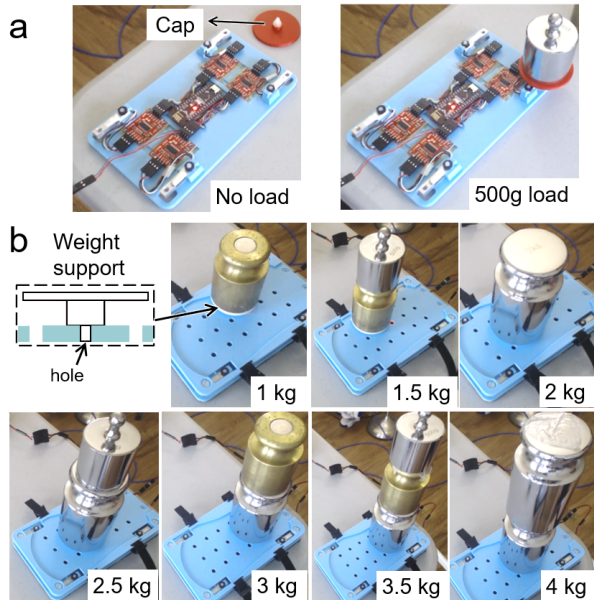


Fig. 3. (a) Load cell calibration. Left and right show data collection with and without load. (b) Shoe manual calibration by applying seven known weights at the holes on the shoe's top plate by a 3-D printed cap.

deviation at the same calibration spot for different applied weights, which has already demonstrated its effectiveness in our previous work [7]. The formulation is the same for Δy in (5). Eventually, a nonlinear least squares is used to minimize the error between the corrected CoP and the ground truth:

$$\operatorname{argmin}_{\zeta} J = \sum_{k=1}^N \|\mathbf{c}_k - \mathbf{p}_k\|^2, \quad (6)$$

where $\zeta = [a_1, \dots, a_3, m_1, \dots, m_4, b_1, \dots, b_3, n_1, \dots, n_4]$ in (5).

C. Shoe measurement accuracy

Mean absolute error (MAE) is used to quantify the CoP and GRF accuracy. The MAE of the GRF, e_G , is given by:

$$e_G = \left(\sum_{k=1}^N |f_z[k] - G_{\text{weight}}[k]| \right) / N, \quad (7)$$

where N and k are sample index and number. f_z is the measured GRF and G_{weight} is the weight of the mass. The

MAE of CoP, e_C , is defined as:

$$e_C = \left(\sum_{k=1}^N \|\mathbf{c}(k) - \mathbf{t}(k)\| \right) / N, \quad (8)$$

where \mathbf{c} and \mathbf{t} are the measured CoP and the ground truth.

The visualizations of the measured GRF and CoP are shown in Fig. 2. Their detailed MAEs are listed in Table I. According to the results, the measured GRF (Fig. 2a, blue circles) almost lie perfectly on their corresponding ground truths (Fig. 2a, black lines) with the MAE only around 0.03N (Table I); The corrected CoPs (Fig. 2b, left, colored markers) become much closer to their corresponding ground truth (Fig. 2b and c, gray circles) compared with the initial measurements (Fig. 2c, left, colored markers). The accuracy of the corrected CoPs is improved about five times (Table I) with only around 1 mm MAE (Table I). The results indicate that manual calibration enables high CoP measurement accuracy for force-sensing shoes. The shoe's accurate GRF and CoP are used to establish ground truth to evaluate the self-calibration.

TABLE I
MANUAL CALIBRATION (MAE)

Shoe	Measured GRF (N)	Measured CoP (mm)	Corrected CoP (mm)
Left	0.02 ± 0.01	4.53 ± 1.89	1.07 ± 0.62
Right	0.03 ± 0.03	3.51 ± 1.90	0.76 ± 0.35

IV. FORCE-SENSING SHOE SELF-CALIBRATION

A. Method overview

When a humanoid robot is in a static configuration, the following relationships hold: **1.** The robot's CoM is modeled by averaging its link CoM positions weighted by the link masses, which is a function of the robot's joint angles:

$$\mathbf{C} = \sum_{i=1}^N \mathbf{c}(\mathbf{q})[i]m[i] / \sum_{i=1}^N m[i], \quad (9)$$

where N and i denote the robot's link number and index; \mathbf{C} is the modeled CoP. \mathbf{c} and m are the CoM and mass of the link. \mathbf{q} is the joint angle vector. **2.** The ground projection of the robot's CoM is the robot's CoP [11]. **3.** The robot's normal GRF equals its weight. **4.** The measured CoP

and normal GRF using sensor parameters (see Section III-B) approximately equals the modeled CoP and the robot's weight.

With the above established relationships, we design the self-calibration method by letting the robot reach different static configurations and then minimizing the error between the measured GRF, CoP and their corresponding modeled references over sensor parameters through optimization.

B. Robot Configuration Sampling

To sample static configurations, we considered two options: **1.** *The robot stands with single support and self-calibrate each shoe separately.* **2.** *The robot stands with double support and self-calibrate both shoes together.* The former is ideal since it focuses on only four sensors in one shoe, which reduces the chances of over-fitting in the optimization. However, the single support option requires the robot to reach many configurations with only one foot supporting its weight. This process will result in excessive torque for smaller-sized humanoid robots with under-powered motors. In addition, our NAO platform encountered serious ankle overheating issues standing in single support in different configurations during initial testing. Therefore, the double support option is chosen for safety concerns.

When calibrating eight sensors in both feet, each sensor's voltage variation should cover a sufficient range to prevent overfitting. Furthermore, a significant amount of data is required for the training process. Two strategies are developed to increase the effectiveness of data sampling. **1.** Sampling double supports with sufficient difference in their position and orientation (see Section V-A for detail). **2.** Instead of shifting to different double supports continuously, the robot moves slowly (close to quasi-static) in each double support and drives its CoP to different areas of the sensing polygon (see Section V-B for detail). These strategies ensure all the sensors are well activated and enough samples are collected.

V. MOTION PLANNING

This section introduces the detailed sampling and planning methods to achieve the two abovementioned strategies.

A. Double support configuration generation

Each double support configuration is defined using the position and orientation of one shoe relative to another using three parameters: $[\Delta x, \Delta y, \Delta \theta]$ (Fig. 4a). We first discretize these parameters in the robot's factory allowable ranges (Fig. 4a, blue area) and then randomly sample in the discretized space. For each sample, a collision check is implemented to ensure no collision occurs and a configuration distance check is performed to ensure all samples are sufficiently different. The configuration distance metric is designed as:

$$d_{SE(2)} = w_d \sqrt{\Delta x^2 + \Delta y^2} + w_o |\Delta \theta|, \quad (10)$$

where w_d and w_o are the weights of the Cartesian distance and the relative orientation. Once the newly sampled double support passes both checks, it is stored for later execution.

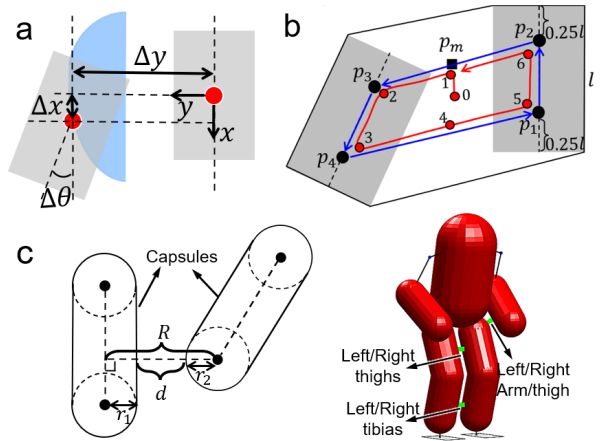


Fig. 4. (a) The configuration of the double support (grey rectangles) are defined with Δx , Δy and $\Delta \theta$. Blue region shows the factory allowable position of one foot relative to another. (b) CoP trajectory generation. $p_1 - p_4$ are the CoP landmarks. Blue and red curves show the modeled CoP trajectory and its reference polygon defined using landmarks. point 0 is the initial CoP position and p_m is the initial target for the modeled CoP. (c) left: the schematic showing the minimal distance between two 3-D capsules, where r_1, r_2 are the radii of the collision pairs, d and R are the minimal distance between the capsules and their centerlines.

B. Whole-body trajectory generation

For each sampled double support, a whole-body trajectory is generated based on the following steps. First, four CoP landmarks are designed at the sensing polygon's centerlines and are 0.25-length away from the sensing polygon's front or rear edges (Fig. 4b, $p_1 - p_4$). Then a trajectory planner generates a series of joint angle vectors, enabling the modeled CoP (Fig. 4b, red curve) to move counter-clockwise along the polygon contour constructed by the landmarks (Fig. 4b, blue curve). Initially, the CoP is driven towards one of the midpoints (Fig. 4b, p_m) of the polygon contour that is closest to the robot's initial CoP (Fig. 4b, point 0). The robot's arms are fixed in the trajectory, as they have little impact on CoP.

We adopt the direct collocation technique [24] for trajectory optimization because it effectively solves trajectory including complex path constraints like our case. The optimization is formulated as:

$$\underset{\mathbf{u}, \mathbf{q}}{\text{minimize}} \quad \sum_{i=1}^N (||\mathbf{c}[i] - \mathbf{c}_{\text{ref}}||_{Q_c}^2 + ||\mathbf{u}[i] - \mathbf{u}[i-1]||_{Q_u}^2) \quad (11)$$

$$\text{subject to:} \quad \mathbf{q}[i] = \mathbf{q}[i-1] + \mathbf{u}[i-1] \quad (\text{State}) \quad (12)$$

$$\mathbf{c}[i] = \text{CoP}(\mathbf{q}[i]) \in \text{SP} \quad (\text{stability}) \quad (13)$$

$$\mathbf{q}_{\min} < \mathbf{q}[i] < \mathbf{q}_{\max} \quad (\text{Joint limit}) \quad (14)$$

$$\mathbf{d}[i] = \text{Dist}(\mathbf{q}[i]) > \mathbf{d}_{\min} \quad (\text{Collision}) \quad (15)$$

$$\mathbf{T}[i] = \text{TF}(\mathbf{q}[i]) = \mathbf{T}_0 \quad (\text{Foot TF}) \quad (16)$$

where the system states are a series of joint angle vectors: $\mathbf{q} = [\mathbf{q}_1, \dots, \mathbf{q}_N]$. Since the robot is assumed to move quasi-statically, the control of the system, $\mathbf{u} = [\mathbf{u}_1, \dots, \mathbf{u}_{N-1}]$, is defined as a series of vectors connecting two consecutive states (12). The cost function (11) penalizes the distance between the modeled CoP $\mathbf{c}[i]$ and the CoP landmark \mathbf{c}_{ref} to drive the CoP trajectory towards each landmark. Moreover,

Algorithm 1 Trajectory planning

Command robot to reach the sampled double support
Measure robot’s configuration using encoders
 $n \leftarrow 1$ (Assign CoP landmark index)
 $s \leftarrow 0$ (Assign planner step)
 $\mathbf{c}_{\text{dist}}[s] \leftarrow \|\mathbf{c}_s - \mathbf{c}_n\|$ (Assign CoP to landmark distance)
while $n < N$ **do**
 Run optimizer (11–16)
 $s \leftarrow s + 1$
 $\mathbf{c}_{\text{dist}}[s] \leftarrow \|\mathbf{c}_s - \mathbf{c}_n\|$
 if $\|\mathbf{c}_s - \mathbf{c}_n\| < r$ or $\mathbf{c}_{\text{dist}}[s - 1] - \mathbf{c}_{\text{dist}}[s] < 0$ **then**
 $n \leftarrow n + 1$
 end if
end while

the cost (11) also minimizes the control difference to smooth the trajectory. Several path constraints are imposed: the stability constraint (13) confines the modeled CoP inside the sensing polygon of the double support. The joint angle limit constraint (14) determines the lower and upper bound of the system states. To formulate the collision constraints (15), 3-D capsules are used to approximate the robot’s links (Fig. 4c, left). The constraints limit the minimal distance between capsules to be greater than zero, where the minimal distance is obtained using the distance between the capsules’ centerlines (Fig. 4c, left, R) to subtract the sum of the capsules’ radii (Fig. 4c, left, r_1 and r_2). The collision pairs to be checked are shown in (Fig. 4c, right). The foot transformation constraint (16) preserves the relative position and orientation between the feet for all the states in the trajectory. Finally, the optimization is solved using a sequential quadratic programming solver. In practice, it is challenging for the solver to generate a complete trajectory directly connecting adjacent CoP landmarks for different double supports. On the one hand, the convergence of the optimizer is sensitive to the number of states in the trajectory. On the other hand, a feasible trajectory may not exist once the robot’s configuration gets closer to its singularity, which occurs when the CoP is close to its landmark. To ensure our algorithm runs autonomously, the planner is implemented in a model predictive control scheme: the optimizer continuously generates a small portion of the trajectory ahead of time, moving the CoP towards its landmark. Once the CoP is close enough to the landmark, or the CoP trajectory cannot proceed towards the landmark, the next landmark is updated. The detailed implementation of the planner is presented in Algorithm 1 and the snapshots of the generated trajectories are shown in Fig. 7 and 8.

VI. IMPLEMENTATION DETAILS

A. Data preparation

To implement our self-calibration algorithm, we sampled five different double supports and then generated their corresponding whole-body trajectories. Among these datasets, three are randomly chosen for training purpose (Fig. 7). The

TABLE II
GRF & CoP MEAN ABSOLUTE ERROR (UNIT: N)

	data 1	data 2	data 3	data 4	data 5
GRF (N)	0.27 ± 0.22	0.27 ± 0.20	0.12 ± 0.16	0.25 ± 0.21	0.31 ± 0.16
CoP (mm)	2.98 ± 1.62	2.72 ± 1.37	2.20 ± 1.19	2.50 ± 1.71	2.01 ± 1.56

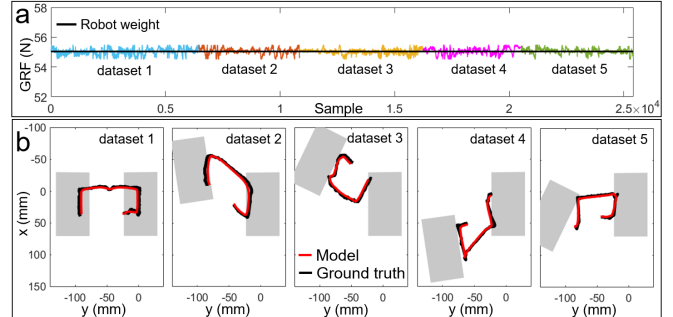


Fig. 5. (a) Quasi-static assumption evaluation. Black line represents the robot’s weight and the colored lines represent the measured GRF using manual calibration for the five sampled datasets. (b) Comparison between modeled CoPs and their corresponding ground truth using manual calibration. Grey rectangles show the sensing polygon of each foot. Black and red curves show the CoP ground truth and the modeled CoP.

other two (Fig. 8) are used to evaluate the performance of the self-calibration algorithm.

B. Modeling reliability

For self-calibration to work effectively, two assumptions need to be tested. **Assumption 1:** The robot’s slow movement can be modeled as a quasi-static system. **Assumption 2:** The modeled CoP is sufficiently close to the ground truth. To test these two assumptions, we manually calibrated the shoes and use their high-accurate measurements (see Table I) as ground truths to evaluate the modeled results. For Assumption 1, we compared the measured normal GRF using manual calibration and the robot’s weight. For Assumption 2, we compared the modeled CoP and the measured CoP using manual calibration for all generated trajectories. The comparison of the GRF and CoP are shown in Fig. 5a, b and their MAEs are shown in Table II. The results show that the measured GRF slightly oscillates around the ground truth (Fig. 5a) with a small averaged amplitude of around 0.3 N (Table II), indicating that the robot’s slow movement is close enough to the quasi-static condition. In addition, the modeled CoP trajectories are close to the measured references (Fig. 5b) with less than 3 mm averaged error compared to the manual calibrated CoP results (Table II), indicating that the modeling is with decent fidelity. The experimental results prove that both assumptions are practically applicable.

C. Obtaining sensor initial parameters

Our self-calibration utilizes nonlinear least squares to determine the sensor parameters, requiring a reasonable initial guess for each sensor (see Section VI-D). Since all load cells are of the same type, we apply the same initial guess $[c_0, d_0]$ (see Section III-A for sensor modeling) to all the sensors.

Assuming the measured GRF and CoP using initial guess approximately equal their modeled references, the following equations hold:

$$\begin{bmatrix} G_r \\ c_x \\ c_y \end{bmatrix} \approx \begin{bmatrix} \sum_{i=1}^8 (c_0 S[i] + d_0) \\ \sum_{i=1}^8 (c_0 S[i] + d_0) t_x[i] / \sum_{i=1}^8 (c_0 S[i] + d_0) \\ \sum_{i=1}^8 (c_0 S[i] + d_0) t_y[i] / \sum_{i=1}^8 (c_0 S[i] + d_0) \end{bmatrix}. \quad (17)$$

The left side consists of the robot's weight, G_r , and the modeled CoP, $[c_x, c_y]^T$. The right side consists of the measured GRF and CoP, where i is the sensor index, S and (t_x, t_y) are the sensor voltage output and location. As we rearrange the equation to include more training samples, the following equations hold:

$$\begin{bmatrix} \vdots \\ c_x[k]G_r \\ c_y[k]G_r \\ \vdots \end{bmatrix} \approx \begin{bmatrix} \vdots & \vdots \\ \sum_{i=1}^8 S[k][i]t_x[i] & \sum_{i=1}^8 t_x[i] \\ \sum_{i=1}^8 S[k][i]t_y[i] & \sum_{i=1}^8 t_y[i] \\ \vdots & \vdots \end{bmatrix} \begin{bmatrix} c_0 \\ d_0 \end{bmatrix} \quad (18)$$

where k is the sample number. Therefore, the optimal initial guess (c_0, d_0) can be solve by least squares regression.

D. Sensor parameter self-calibration

1) *Loadcell parameter identification*: Given training samples involving sensor voltage outputs and their corresponding modeled GRFs and CoPs (Fig. 7), the load cells' parameters are determined by minimizing the differences between these corresponding pairs using nonlinear least squares (NLS). The optimization variables $\zeta = [(c_1, d_1), \dots, (c_8, d_8)]$ are the parameters of the load cells' scaling factors and offsets in (3). The NLS is formulated as:

$$\underset{\zeta}{\operatorname{argmin}} J = \sum_{k=1}^N (\|n[k] - G_{\text{robot}}\|_{w_n}^2 + \|c[k] - c_m[k]\|_{w_c}^2) + \|\zeta - \zeta_0\|_{w_\zeta}^2, \quad (19)$$

where k is the number of training samples, n and c are measured GRF and CoP; c_m is the modeled CoP (9); G_{robot} is the robot's weight; ζ_0 is the initial guess solved in (18). w_n , w_c and w_ζ are the weights for the cost terms. The regulation term is designed to avoid overfitting.

2) *CoP measurement calibration*: Similar to the manual calibration method (see Section III-B), we further improve the CoP measurement by first defining a corrected CoP:

$$\mathbf{c}_{\text{aug}} = \frac{(\mathbf{c}_L + \Delta \mathbf{s}_L)n_L + (\mathbf{c}_R + \Delta \mathbf{s}_R)n_R}{n_L + n_R}, \quad (20)$$

where c_L , c_R , n_L and n_R are the measured CoP and GRF using sensor parameters solved by (19) for the left and right feet. Δs_L and Δs_R are the correction terms applied to the left and right feet defined in (5). Then we use NLS to minimize the error between corrected and modeled CoPs over the parameters of the correction terms:

$$\underset{\zeta}{\operatorname{argmin}} J = \sum_{k=1}^N (\|c_{\text{aug}}[k] - c_m[k]\|^2), \quad (21)$$

where c_m is the modeled CoP and ζ are the parameters of the correction terms defined in (5).

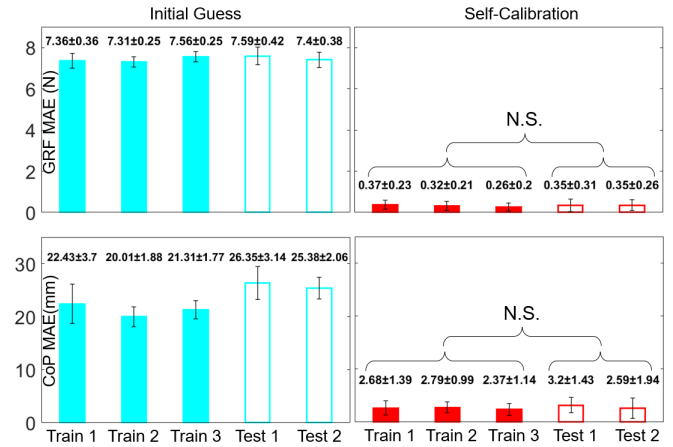


Fig. 6. Top and bottom show the MAE of the measured GRF and CoP using initial guess (left) and self-calibration (right). Filled and empty bars show the training and testing results. N.S means no statistical difference.

VII. RESULT

The measurement results and the ground truths (manual calibration) of the training and testing datasets are shown in Fig. 7 and 8 and the MAE between the measurements and the ground truths are presented in Fig. 6. The results show that GRF and CoP measurements using initial guess (Fig. 7 and Fig. 8, teal lines) are far away from their ground truths (blue lines), with about 7.5 N MAE for GRF and 23 mm MAE for CoP (Fig. 6, left). By contrast, the measurement using self-calibration (Fig. 7 and Fig. 8, red lines) are much closer to their corresponding ground truths (Fig. 7 and Fig. 8, blue lines) with only approximate 0.35 N MAE for GRF and 2.8 mm MAE for CoP. The self-calibration improve the measurements using initial guess by approximately ten times for CoP (Fig. 6, bottom) and 20 times for GRF (Fig. 6, top). In addition, statistical tests show that the training and testing MAEs are not significantly different (Fig. 6, right), indicating no overfitting takes place. The overall results demonstrate that our self-calibration approach can effectively determine sensor parameters without any manual intervention and does not require sensors' information.

VIII. DISCUSSION AND FUTURE WORK

This letter presents a novel self-calibration method for humanoid robots to determine the sensor parameters of their foot force-sensing modules autonomously. This method does not require the information of the sensor's initial parameters and any manual intervention, which can be applied for long-term autonomous tasks. Although the self-calibration approach is demonstrated on our force-sensing shoes designed for smaller humanoid robots, it can theoretically be applied to larger humanoid robots with F/T sensors as well, which requires the same planning and optimization method between the measurements and the modeled references.

Compared with the ground truth produced by manual calibrated sensor parameters (Table I), the measurement using self-calibration is slight off (Fig. 6), which results from the following issues: 1. the robot's movement can never reach

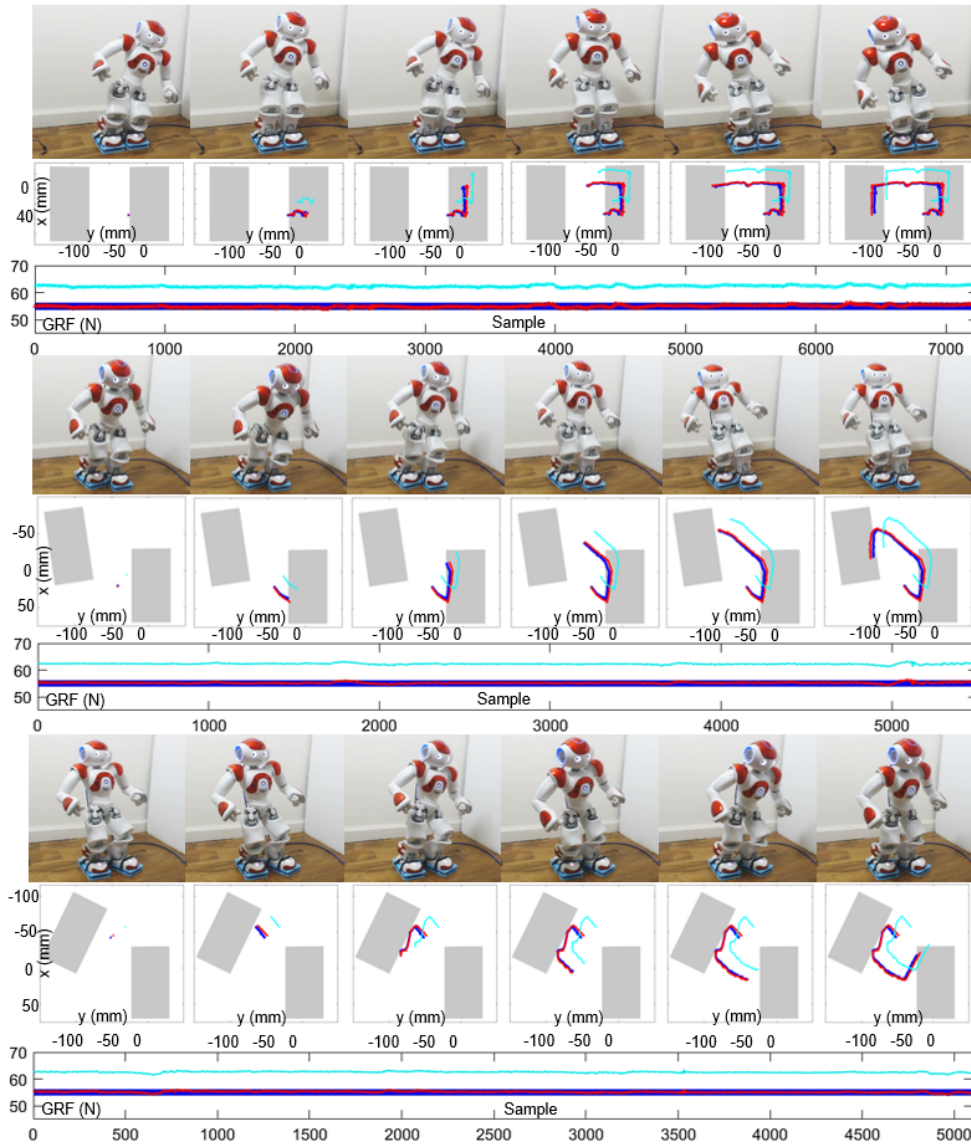


Fig. 7. Three training datasets. Top, middle and bottom sections for each dataset show the evolution of the robot’s motion, its CoP and GRF. Teal, blue and red lines show the measurements using the initial guess, the ground truth and the self-calibration.

fully quasi-static since it generates acceleration when moving along the trajectories. 2. The modeled CoP using the robot’s joint angles does not equal the ground truth perfectly (Table II), resulting in fitting errors in the optimization process. Our future work will address the second issue by further calibrating the robot’s mass properties using a high-accurate commercial force plate to improve the modeling accuracy. In addition, we will increase training data by sampling more double supports to check if the accuracy of the self-calibration will increase. Lastly, we will test our self-calibration approach in the long-term tasks.

IX. ACKNOWLEDGEMENT

This work was supported by NUS Startup grants R-265-000-665-133, R-265-000-665-731, Faculty Board account C-265-000-071-001, and the National Research Foundation,

Singapore under its Medium Sized Center for Advanced Robotics Technology Innovation R-261-521-002-592.

REFERENCES

- [1] M. Vukobratović and B. Borovac, “Zero-moment point—thirty five years of its life,” *International journal of humanoid robotics*, vol. 1, no. 01, pp. 157–173, 2004.
- [2] S. Tsuchihiro, M. Koeda, S. Sugiyama, and T. Yoshikawa, “A sliding walk method for humanoid robots using zmp feedback control,” in *2011 IEEE International Conference on Robotics and Biomimetics*. IEEE, 2011, pp. 275–280.
- [3] S. Nakaura, M. Sampei *et al.*, “Balance control analysis of humanoid robot based on zmp feedback control,” in *IEEE/RSJ International Conference on Intelligent Robots and Systems*, vol. 3. IEEE, 2002, pp. 2437–2442.
- [4] P. Ghassemi, M. T. Masouleh, and A. Kalhor, “Push recovery for nao humanoid robot,” in *2014 Second RSI/ISM International Conference on Robotics and Mechatronics (ICRoM)*. IEEE, 2014, pp. 035–040.
- [5] L. Hawley and W. Suleiman, “External force observer for medium-sized humanoid robots,” in *2016 IEEE-RAS 16th International Conference on Humanoid Robots (Humanoids)*. IEEE, 2016, pp. 366–371.

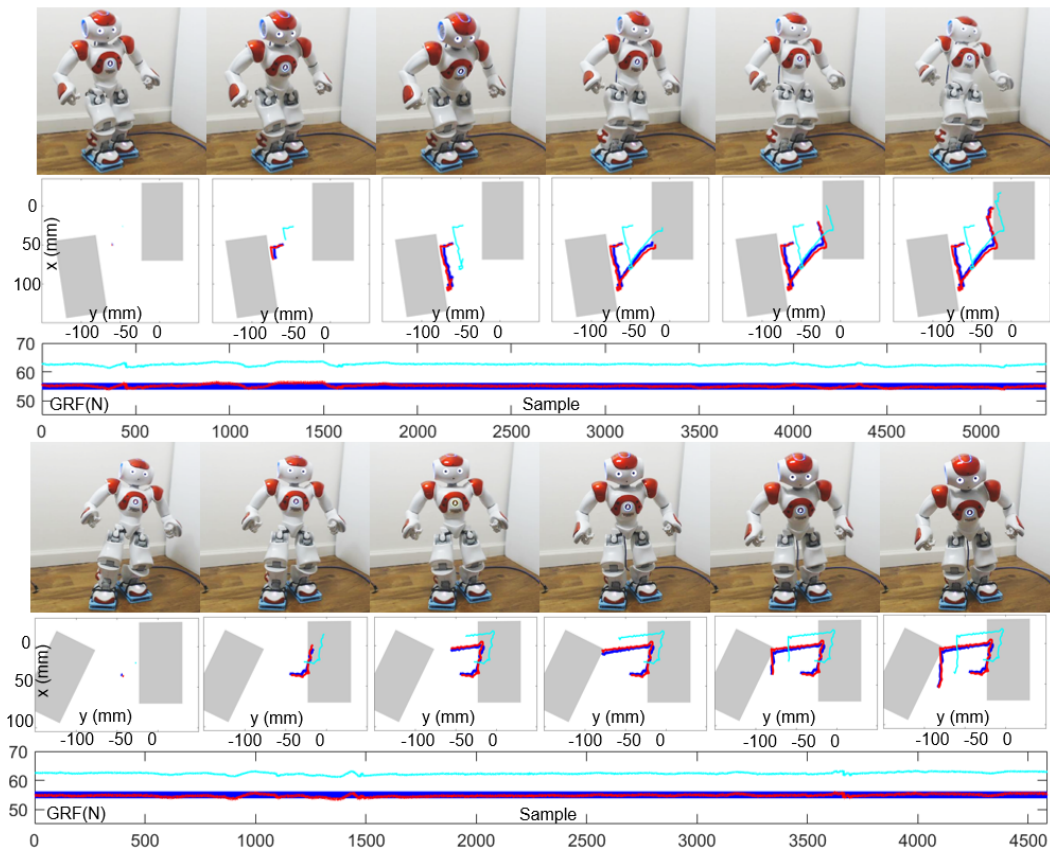


Fig. 8. Two testing datasets. Top and bottom sections for each dataset show the evolution of the robot's motion, its CoP and GRF. Teal, blue and red lines show the measurements using the initial guess, the ground truth and the self-calibration.

- [6] S. Piperakis, M. Koskinopoulou, and P. Trahanias, "Nonlinear state estimation for humanoid robot walking," *IEEE Robotics and Automation Letters*, vol. 3, no. 4, pp. 3347–3354, 2018.
- [7] Y. Han, R. Li, and G. S. Chirikjian, "Can i lift it? humanoid robot reasoning about the feasibility of lifting a heavy box with unknown physical properties," *arXiv preprint arXiv:2008.03801*, 2020.
- [8] R. Shigematsu, S. Komatsu, Y. Kakiuchi, K. Okada, and M. Inaba, "Lifting and carrying an object of unknown mass properties and friction on the head by a humanoid robot," in *2018 IEEE-RAS 18th International Conference on Humanoid Robots (Humanoids)*. IEEE, 2018, pp. 1–9.
- [9] T. Takenaka, "The control system for the honda humanoid robot," *Age and ageing*, vol. 35, no. suppl.2, pp. ii24–ii26, 2006.
- [10] K. H. Koch, K. Mombaur, O. Stasse, and P. Soueres, "Optimization based exploitation of the ankle elasticity of hrp-2 for overstepping large obstacles," in *2014 IEEE-RAS International Conference on Humanoid Robots*. IEEE, 2014, pp. 733–740.
- [11] S. Kajita, H. Hirukawa, K. Harada, and K. Yokoi, *Introduction to humanoid robotics*. Springer, 2014, vol. 101.
- [12] Y. Fujimoto and A. Kawamura, "Attitude control experiments of biped walking robot based on environmental force interaction," in *AMC'98-Coimbra. 1998 5th International Workshop on Advanced Motion Control. Proceedings (Cat. No. 98TH8354)*. IEEE, 1998, pp. 70–75.
- [13] D. Gouaillier, V. Hugel, P. Blazevic, C. Kilner, J. Monceaux, P. Lafourcade, B. Marnier, J. Serre, and B. Maisonnier, "Mechatronic design of nao humanoid," in *2009 IEEE International Conference on Robotics and Automation*. IEEE, 2009, pp. 769–774.
- [14] Y. Takahashi, K. Nishiwaki, S. Kagami, H. Mizoguchi, and H. Inoue, "High-speed pressure sensor grid for humanoid robot foot," in *2005 IEEE/RSJ International Conference on Intelligent Robots and Systems*. IEEE, 2005, pp. 3909–3914.
- [15] B. J. Son, Y. S. Baek, and J. H. Kim, "Development of foot modules of an exoskeleton equipped with multiple sensors for detecting walking phase and intent," in *Applied Mechanics and Materials*, vol. 752. Trans Tech Publ, 2015, pp. 1016–1021.
- [16] A. Hollinger and M. M. Wanderley, "Evaluation of commercial force-sensing resistors," in *Proceedings of the International Conference on New Interfaces for Musical Expression, Paris, France*. Citeseer, 2006, pp. 4–8.
- [17] A. M. Shayan, A. Khazaei, A. Hamed, and M. T. Masouleh, "Design and development of a pressure-sensitive shoe platform for nao h25," in *2019 7th International Conference on Robotics and Mechatronics (ICRoM)*. IEEE, 2019, pp. 223–228.
- [18] H.-J. Kwon, J.-H. Kim, D.-K. Kim, and Y.-H. Kwon, "Fabrication of four-point biped robot foot module based on contact-resistance force sensor and its evaluation," *Journal of mechanical science and technology*, vol. 25, no. 2, p. 543, 2011.
- [19] Y. Han, R. Li, and G. S. Chirikjian, "Look at my new blue force-sensing shoes!" *arXiv preprint arXiv:2104.06618*, 2021.
- [20] L. Almeida, V. Santos, and F. Silva, "A novel wireless instrumented shoe for ground reaction forces analysis in humanoids," in *2018 IEEE International Conference on Autonomous Robot Systems and Competitions (ICARSC)*. IEEE, 2018, pp. 36–41.
- [21] K. Suwanratchatamane, M. Matsumoto, and S. Hashimoto, "Haptic sensing foot system for humanoid robot and ground recognition with one-leg balance," *IEEE Transactions on Industrial Electronics*, vol. 58, no. 8, pp. 3174–3186, 2009.
- [22] "Nao robot's force sensing resistor introduction page," http://doc.aldebaran.com/2-5/family/robots/fsr_robot.html?highlight=fsr.
- [23] G. J. Verkerke, A. Hof, W. Zijlstra, W. Ament, and G. Rakhorst, "Determining the centre of pressure during walking and running using an instrumented treadmill," *Journal of biomechanics*, vol. 38, no. 9, pp. 1881–1885, 2005.
- [24] T. Tsang, D. Himmelblau, and T. F. Edgar, "Optimal control via collocation and non-linear programming," *International Journal of Control*, vol. 21, no. 5, pp. 763–768, 1975.